Chapter 4

Out-of-time-order correlation of the nonlocal block observables in Floquet Ising spin chain

4.1 Introduction

Periodically driven Floquet systems have been extensively studied in the recent past in both classical and quantum systems. A popular set of models are driven by fields applied in the form of kicks [25, 55, 156, 157], as analytical forms of the time evolution operator are easy to find. One textbook example is the kicked-rotor model of a particle moving on a ring [32]. These models show interesting behavior displaying transition from integrability to chaos, dynamical Anderson localization [32, 170, 171], and dynamical stabilization [172, 173]. These systems are of interest in both classical as well as quantum systems. Such periodic forcing has been realized in experiments to study various phenomena [148, 150, 174, 175, 176].

In contrast to the kicked rotor, the Ising model with time-periodic transverse and longitudinal magnetic fields is an example of a many-body Floquet system of current

interest [25, 53, 54, 55]. Absence of a transverse component renders the system trivially integrable. Presence of both a longitudinal and transverse magnetic component makes this system nonintegrable. However, in the absence of longitudinal field, the system is rendered integrable as a system of noninteracting fermions. These systems have been studied using sudden quenches [177], and slow annealing [178]. In the quenched case, the system is out of equilibrium and leads to interesting dynamics of the observables, and has drawn considerable attention in the last decade with significant theoretical and experimental observations [158, 161, 162].

A typical way to distinguish between integrable, non-integrable, and near-integrable regimes has been to use spectral properties and random matrix theory. This mostly leaves aside the question of dynamics. However, a quantity that has been extensively used recently to distinguish the chaotic and integrable dynamics is the out-of-time-order correlator (OTOC) [24, 26, 27, 65, 69, 179]. In classical physics, one hallmark of chaos is that a small difference in the initial condition results in the exponential deviation of the trajectory, which is responsible for the so-called “butterfly effect" [8, 9, 10]. Classical Hamiltonian systems can have such pure deterministic chaos, which is used in the quantum domain for the study of quantum chaos [23, 124]. It has been proposed that quantum chaos be characterized by the growth rate of OTOC [97], an exponential growth defining a quantum Lyapunov exponent.

Spin systems have been a playground for understanding many-body physics in general, and the growth of OTOCs in particular [58, 59, 60, 61, 62, 63, 64, 65, 66, 67, 68, 69]. Growth of OTOC is discussed in systems such as Luttinger liquids [67], XY model [66], Sachdev-Ye-Kitaev (SYK) model [70], Heisenberg XXZ model and Aubry–André–Harper model [68, 69]. Lin and Motrunich [58] calculated OTOC for single spin observables in the integrable transverse field Ising model and observed power-law growth, with the power varying with the separation between the localized spins.

Fortes *et al.* [62] studied OTOCs in the time-independent Ising model with tilted magnetic fields, perturbed XXZ model, and Heisenberg spin model with random magnetic fields. In all these models with single-spin observables, only power-law growth has been reported despite the presence of quantum chaos. OTOCs in integrable and nonintegrable Floquet Ising models were studied by Kukuljan *et al.* [61] using extensive observables. In one dimension case, the growth of OTOC density was still found to be linear in time.

The cases where exponential growth has been definitely reported involve semiclassical models such as the quantum kicked rotor [24], coupled kicked rotors [176, 180], the kicked top, which may be considered to be a transverse field kicked Ising model but with the interactions being all-to-all [181, 182], the bakers map [183], and so on. Our motivation herein is to allow for a large Hilbert space for the observables, which are restricted to blocks of spins. We may consider the spin chain as a bipartite chaotic system, each consisting of $N/2$ spins, to explore the possibility of exponential growth. We will see that such spin-1/2 nonintegrable models, even for block operators, have only power-law OTOC growth, implying that their quantum Lyapunov exponents are 0.

In nonintegrable systems including spin chains such as studied here, the long-time saturation value of the OTOC is consistent with an estimate from random matrix theory. The approach of the OTOC to the saturation value was found to be at an exponential rate in a weakly interacting bipartite chaotic system [180]. Exponential approach to saturation was also found in a semiclassical theory of OTOC [184]. We find such an exponential approach to the random matrix value in spin chains with block observables for the nonintegrable cases.

To understand the exponential approach, we consider the case when the block operators are random. Averaging over random unitary operators in a bipartite system, the OTOC has been shown to be exactly the operator entanglement of the propagator [185]. We show

this is also the case with random Hermitian observables drawn from the Gaussian Unitary Ensemble (GUE).

Thus the exponential saturation of the OTOC is qualitatively consistent with the behavior previously observed for the operator entanglement growth of the propagator [186].

According to the BGS conjecture [72], the spectral properties of the quantum analogue of a chaotic classical system will follow Wigner-Dyson statistics, unlike the quantum analogue of an integrable classical system following Poisson distribution. Thus, the spectral statistics of spacing between the consecutive energy levels of a quantum system works as a tool to differentiate a chaotic system from an integrable one [13, 13, 63, 77, 78, 186, 187, 188].

This chapter is organised as follows. In subsection 4.2.1, we will discuss the Floquet map with and without longitudinal fields. In subsection 4.2.2, we will define the OTOC for the block spin operators. In subsection 4.2.3, we will discuss the relation of OTOC with operator entanglement entropy (OPEE). In subsection 4.2.4, we will elaborate the nearest-neighbor spacing distribution (NNSD) and its behavior in the integrable and nonintegrable cases. We will elaborate the behavior of OTOC and NNSD in section 4.3 for the constant-field Flqouet system, and in section 4.4, a special case of constant-field Flquet system. Finally, in section 4.5, we will conclude the results of this chapter.

4.2 The spin model and background

4.2.1 The spin model

Consider a periodically driven Ising spin system with the Hamiltonian

$$\hat{H}(t) = J_x \hat{H}_{xx} + h_x \hat{H}_x + h_z \sum_{n=-\infty}^{\infty} \delta\left(n - \frac{t}{\tau}\right) \hat{H}_z. \tag{4.1}$$

Here $\hat{H}_{xx} = \sum_{l=1}^{N-1} \hat{\sigma}_l^x \hat{\sigma}_{i+1}^x$ is the nearest-neighbor Ising interaction term, $\hat{H}_x = \sum_{l=1}^{N} \hat{\sigma}_l^x$ and $\hat{H}_z = \sum_{l=1}^{N} \hat{\sigma}_l^z$. The interaction strength is J_x, the continuous and constant longitudinal magnetic field in x-direction is given by h_x and the transverse magnetic field in the z-direction, which is applied in the form of delta pulses at regular interval τ is h_z.

The Floquet operator is the propagator connecting states across one time period τ. Denoting this as $\hat{\mathscr{U}}_x$, we have (with $\hbar = 1$)

$$\hat{\mathscr{U}}_x = \exp\left[-i\tau(J_x\hat{H}_{xx} + h_x\hat{H}_x)\right] \exp\left(-i\tau h_z \hat{H}_z\right), \tag{4.2}$$

and will be referred to as "$\hat{\mathscr{U}}_x$ systems" below, when the longitudinal field is absent, the model is solvable by the Jordan–Wigner transformation and renders the system as one of noninteracting fermions. In the presence of the longitudinal field, these fermions are interacting, and there is evidence that there is a transition to quantum chaos [54, 167, 168, 189, 190]. The Floquet map of the integrable model is a special case of Eq. (3.4) with $h_x = 0$ will be referred to as the $\hat{\mathscr{U}}_0$ system below.

4.2.2 Out-of-time-order correlation and block operators

Dynamics of quantum systems lead to the spreading of initially localized operators under the unitary time evolution. Let the discrete time evolution of operator $\hat{W} \equiv \hat{W}(0)$ be $\hat{W}(n) = \hat{U}(n)^\dagger \hat{W}(0)\hat{U}(n)$, where $\hat{U}(n)$ is time$-n$ propagator. For example, if the time evolution is governed by Eq. (3.4), $\hat{U}(n) = \hat{\mathscr{U}}_x^n$. If $\hat{V}$ and $\hat{W}$ are two Hermitian operators that are localized on different sets of spins (say A and B), we consider as the out-of-time-order correlation (OTOC) [19, 22, 97, 98, 125, 191, 192, 193]:

$$C(n) = -\frac{1}{2\,d_A d_B} \mathrm{Tr}\left([\hat{W}(n), \hat{V}]^2\right), \tag{4.3}$$

where d_A and d_B are dimensions of the subspaces, and $d_A = d_B = 2^{N/2}$ as we consider only the case of equal blocks. The OTOC $C(n)$ is clearly a measure of the non-commutativity of these two operators via its norm.

This separates as $C(n) = C_2(n) - C_4(n)$, where $C_2(n)$ and $C_4(n)$ are two-point and four-point correlations respectively:

$$\begin{aligned} C_2(n) &= \frac{1}{d_A d_B}\mathrm{Tr}(\hat{W}^2(n)\hat{V}^2), \\ C_4(n) &= \frac{1}{d_A d_B}\mathrm{Tr}(\hat{W}(n)\hat{V}\hat{W}(n)\hat{V}). \end{aligned} \tag{4.4}$$

These are infinite temperature quantities and involve the entire spectrum of 2^N states. We will use the trick of evaluating this by employing Haar random states of 2^N dimensions to evaluate expectation values, that is $\mathrm{Tr}(\hat{A})/2^N \approx \langle \Psi_R|\hat{A}|\Psi_R\rangle$ were $|\Psi_R\rangle$ is such a state. Averages over a few random states are used.

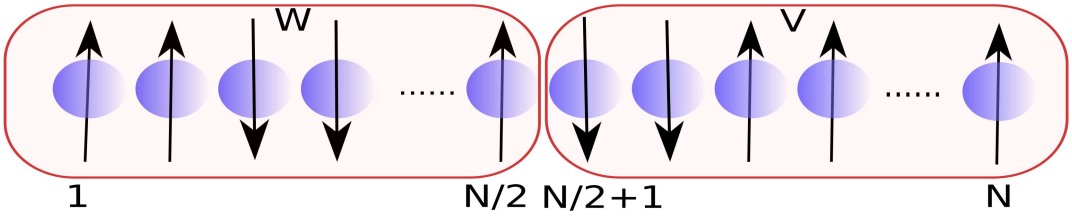

Fig. 4.1 Schematics of SBOs defined in Eq. (4.5). Even N is considered and halved into subsystems W and V.

Almost all studies of OTOC in such spin models thus far concentrate on operators that are localized on single spins, in contrast, we consider operators $\hat{V}$ and $\hat{W}$ initially isolated on the first and second block of spins, see Fig. 4.1, referred to here as spin-block-operators (SBOs):

$$\hat{W} = \frac{2}{N}\sum_{l=1}^{\frac{N}{2}} \hat{\sigma}_l^x \quad \text{and} \quad \hat{V} = \frac{2}{N}\sum_{l=\frac{N}{2}+1}^{N} \hat{\sigma}_l^x. \tag{4.5}$$

Note that the behavior of these OTOCs is genuinely different and does not follow from a knowledge of the single site OTOCs involving correlations such as $\langle \hat{\sigma}^x_{l_1}\, \hat{\sigma}^x_{l_2}(n)\, \hat{\sigma}^x_{l_3}\, \hat{\sigma}^x_{l_4}(n)\rangle$ for general values of l_i.

For $n > 0$, $\hat{W}(n)$ is no longer confined to the first $N/2$ spins, and the OTOC becomes nonzero. Previous studies with single-site localized observables show no exponential growth of OTOC even for nonintegrable cases in such spin models. The cases where exponential growth has been definitely reported involve semiclassical models such as the quantum kicked rotor, coupled kicked rotors, the kicked top wherein the interactions are all-to-all, the bakers map, and so on. Our motivation herein is to allow for a large Hilbert space for the local operators. We may consider the spin chain as a bipartite chaotic system, each consisting of $N/2$ spins, to explore the possibility of exponential growth.

If short-time growth is exponential [14, 24, 26, 188] then it is related to quantum chaos and quantum Lyapunov exponents. Can the OTOC help define a quantum Lyapunov exponent for spin models with short-range interactions such as in Eq. (3.4)? Integrable system show power-law growth of OTOC before the scrambling time [14, 24, 26, 58, 62, 188]. However, it is unclear under what circumstances OTOC of nonintegrable systems with other signatures of quantum chaos can fail to grow exponentially. We will see that such spin-1/2 nonintegrable models continue even for block operators to not have an unambiguous exponential OTOC growth.

4.2.3 Average and asymptotic OTOC values

As $\hat{V}$ and $\hat{W}$ are block restricted sums of spin operators, $\hat{V}+\hat{W}$ is the total spin in the x direction and appears as a term in the Hamiltonian. Thus these are special operators with dynamical significance, as would be natural to assume. In contrast, if they are random operators on the space of $N/2$ spins, the OTOC behaves quite differently till possibly the scrambling time. Beyond the scrambling time, we may expect that the local operators

have largely become random if there is nonintegrability and quantum chaos. Thus, it is of interest to compare the behavior of random operator OTOC with non-random ones: to separate the effects of dynamics and scrambling. In a semiclassical model of weakly coupled chaotic systems, it was noted that the post-scrambling time OTOC of non-random operators did behave as that of “pre-scrambled" random operators [180]. We find some similarities in the case of spin chains but also interesting differences.

In the case of random operators for $\hat{V}$ and $\hat{W}$, ergodicity may be expected and hence an average over them is done. It has been observed [194] that if these operators are random unitaries chosen uniformly (Haar measure, circular unitary ensemble, CUE), the average OTOC is remarkably related to the operator entanglement. As we are using Hermitian operators, we average over random Hermitian ensembles for which we naturally choose the GUE, and the result is identical.

Let there be a bipartite space $\hat{\mathscr{H}}_A \otimes \hat{\mathscr{H}}_B$, such as the space of the first and second $N/2$ spins in the chain. The Schmidt decomposition of the unitary propagator on this bipartition is of the form

$$\hat{U}(n) = 2^{N/2} \sum_{i=1}^{2^N} \sqrt{\lambda_i(n)} \hat{A}_i(n) \otimes \hat{B}_i(n). \tag{4.6}$$

Here $\hat{A}_i(n)$ and $\hat{B}_i(n)$ are orthonormal operators on individual spaces $\hat{\mathscr{H}}_{A,B}$, satisfying, $\mathrm{Tr}(\hat{A}_i(n)^\dagger \hat{A}_j(n)) = \mathrm{Tr}(\hat{B}_i(n)^\dagger \hat{B}_j(n)) = \delta_{ij}$. The numbers $\lambda_i(n) > 0$ satisfy the condition $\sum_i \lambda_i(n) = 1$ which is a consequence of the unitarity of $\hat{U}(n)$.

Operator entanglement entropy (OPEE) is used for the measure of entanglement [186, 194, 195, 196] and defined via the linear entropy as

$$E_l[\hat{U}(n)] = 1 - \sum_{i=1}^{2^N} \lambda_i^2(n). \tag{4.7}$$

This vanishes if and only if $\hat{U}(n)$ is of product form and is maximum when all $\lambda_i(n) = 2^{-N}$ and the OPEE is equal to $1 - 2^{-N}$.

Let an element of the GUE be $\hat{W} = (\hat{M} + \hat{M}^\dagger)/2$, where $\hat{M}$ is a d dimensional matrix whose entries are such that its real and imaginary parts are zero centered, unit variance, independent normal random numbers, the Ginibre ensemble. It is straightforward to see that $\overline{\hat{W}^2} = d\,\hat{I}_d$, where $\hat{I}_d$ is the d dimensional identity matrix, and the overline indicates the GUE average. The average of $C_2(n)$ is then

$$\overline{C_2(n)}^{\hat{W},\hat{V}} = \frac{1}{d^2}\overline{\mathrm{Tr}\left(\hat{U}(n)^\dagger \hat{W}^2 \hat{U}(n) \hat{V}^2\right)}^{\hat{W},\hat{V}} = d^2, \tag{4.8}$$

where $\hat{V}$ is also a GUE realization independent of $\hat{W}$.

To evaluate the 4-point function $C_4(n)$, we need to use the standard ploy of doubling the space: $\mathrm{Tr}(\hat{A}^2) = \mathrm{Tr}((\hat{A} \otimes \hat{A})\,\hat{S})$ where $\hat{S}$ swaps the original and ancilla spaces. With $\hat{A} = \hat{W}(n)\hat{V}$. The only relevant average needed is

$$\overline{\hat{W} \otimes \hat{W}}^{\hat{W}} = \hat{S}, \tag{4.9}$$

and it follows using identities known for the operator entanglement [185, 194] that $\overline{C_4(n)}^{\hat{W},\hat{V}} = d^2[1 - E_l(\hat{U}(n))]$ and hence the OTOC averaged over the observables is

$$\overline{C(n)}^{\hat{W},\hat{V}} = d^2 E_l[\hat{U}(n)]. \tag{4.10}$$

Thus the observable averaged OTOC is identical to the OPEE. Based on ergodicity, the case of a single random realization may then be expected to be represented by this average.

In the asymptotic limit of large times, if the dynamics are chaotic, we may expect that $\hat{U}(n)$ is a complex operator on the whole Hilbert space and treat it as being sampled according to the random CUE of size 2^N while keeping the $\hat{W}$ and $\hat{V}$ as fixed or non-random operators. The averaged quantities for traceless operators $\hat{V}$ and $\hat{W}$ are (see Appendix C-I

for details)

$$\overline{C_2(n)}^U = \frac{1}{d^2}\mathrm{Tr}(\hat{W}^2)\mathrm{Tr}(\hat{V}^2) \tag{4.11a}$$

$$\overline{C_4(n)}^U = \frac{-1}{d^2(d^2-1)}\mathrm{Tr}(\hat{W}^2)\mathrm{Tr}(\hat{V}^2) \tag{4.11b}$$

$$\overline{C(n)}^U = \frac{1}{d^2-1}\mathrm{Tr}(\hat{W}^2)\mathrm{Tr}(\hat{V}^2). \tag{4.11c}$$

For the $\hat{W}$ and $\hat{V}$ in Eq. (4.5), the asymptotic value of the OTOC, ignoring the C_4 value, which is of lower order in the Hilbert space dimension, is this average and denoted below as

$$C(\infty) = 4/N^2. \tag{4.12}$$

For the GUE random $\hat{V}$ and $\hat{W}$ used above $\overline{\mathrm{Tr}\hat{W}^2} = d^2$ and hence in this case $C(\infty) = d^2 = 2^{2N}$ for large d. We will always study scaled OTOC, dividing by the relevant $C(\infty)$; thus for the random operator case, the averaged and scaled OTOC is exactly the OPEE $E_l[\hat{U}(n)]$.

4.2.4 Nearest-neighbour spacing distribution

Spectral statistics of the spacing between consecutive energy levels are used to differentiate the chaotic and integrable regimes. In order to calculate the NNSD, first, we need to identify the symmetries of the Hamiltonian. Next, the Hamiltonian is block diagonalized in the symmetry sectors. Our system with open boundary conditions has a "bit-reversal" symmetry at all the Floquet periods. This bit-reversal symmetry is due to the fact that the field and interaction do not distinguish the spins by interchanging the spins at the sites i and $N-i+1$ for all $i = 1, \cdots, N$. Let us consider $\hat{B}$ a bit-reversal operator given by

$$\hat{B}|\mathtt{s}_1, \mathtt{s}_2, \cdots, \mathtt{s}_N\rangle = |\mathtt{s}_N, \cdots, \mathtt{s}_2, \mathtt{s}_1\rangle, \quad [\hat{U}, \hat{B}] = 0,$$

where $|\mathtt{s}_i\rangle$ is any single-particle basis state in standard $(\mathtt{s}_z)$ basis. We divide whole basis sets into two groups of basis states, one with the palindrome in which there is no change in the state after applying the operator $\hat{B}$ *i.e.*, $\hat{B}|\mathtt{s}_1,\mathtt{s}_2,\cdots,\mathtt{s}_N\rangle = |\mathtt{s}_1,\mathtt{s}_2,\cdots,\mathtt{s}_N\rangle$. The other one with the non-palindrome in which states get reflected after applying the operator $\hat{B}$ *i.e.* $\hat{B}|\mathtt{s}_1,\mathtt{s}_2,\cdots,\mathtt{s}_N\rangle = |\mathtt{s}_N,\cdots,\mathtt{s}_2,\mathtt{s}_1\rangle$. Since $\hat{B}^2 = 1$, the eigenvalues of $\hat{B}$ are ± 1. The eigenstates can be classified as odd or even states under bit reversal. All the palindromes are even states; however, all the non-palindromes have one even and one odd state. Sum and difference of the non-palindrome and its reflection generate even and odd states. The dimension of the odd subspace is equal to half the number of non-palindromic binary words of length N, *i.e.*, $\frac{1}{2}\left(2^N - 2^{\frac{N}{2}}\right)$, while the even subspace is equal to the sum of half the number of palindromic bit sequences and half the number of total space of the same length *i.e.* $\frac{1}{2}\left(2^N + 2^{\frac{N}{2}}\right)$.

In the NNSD, it is necessary to concentrate on the fluctuations properties of the spectrum, which display universal effects. For this, one should do the unfolding of the spectrum in order to get rid of the non-universal properties (level density). Unfolding is usually done by parameterizing numerically obtained level densities in terms of a smooth function, typically a polynomial, followed by mapping the energies to unfolded ones such that the mean energy spacing is unity.

We consider the ensemble of differences between the consecutive energy levels. The average spacing between the consecutive eigenvalues is controlled by the local mean density of states. If within a region δE of the spectrum, there are $D(E)\delta E$ eigenvalues, then the average spacing between the consecutive eigenvalues will be $1/D(E)$. If we re-scale the differences between the consecutive eigenvalues by the local mean density of states, the average difference will be one. We study the shape of distribution by using the NNSD, which may be used as an indicator of quantum chaos and nontrivial integrable models.

In NNSD, strongly chaotic points are those where the unfolded level-spacings are well described by the Wigner distribution [76, 77, 78] which is given as

$$P_W(s) = \frac{\pi s}{2} e^{-\pi s^2/4}, \tag{4.13}$$

where s is drawn from the ensemble of consecutive energy level separation. On the other hand, nontrivial integrable models are those where the unfolded NNSD follows Poisson statistics,

$$P_P(s) = e^{-s}. \tag{4.14}$$

4.3 Constant field Floquet system

We analyze the OTOC given by Eq. (4.3) for integrable $\hat{\mathscr{U}}_0$ and nonintegrable $\hat{\mathscr{U}}_x$ systems defined in section 4.2.1. The Floquet period τ acts as a parameter to drive the system into interesting dynamical regimes. In this chapter, we will discuss the dynamic (pre-Ehrenfest time) and saturation (post-Ehrenfest time) regions of OTOC generated by SBOs defined in Eq. (4.5). We will only focus on the behavior of OTOC in the range of Floquet periods from 0 to $\frac{\pi}{4}$ as OTOCs for our Floquet systems $\hat{\mathscr{U}}_0$ and $\hat{\mathscr{U}}_x$ are exactly the same for τ and $\frac{\pi}{2} - \tau$. This peculiarity of OTOC can be shown below by taking $J_x = 1$, $h_x = h_z = 4$ and replacing τ by $\frac{\pi}{2} - \tau$ in Eq. (3.4).

$$\begin{aligned}
\hat{\mathscr{U}}_x\left(\frac{\pi}{2} - \tau\right) &= e^{-i(\hat{H}_{xx}+4\hat{H}_x)(\frac{\pi}{2}-\tau)} e^{-i4\hat{H}_z(\frac{\pi}{2}-\tau)}, \\
&= e^{i(\hat{H}_{xx}+4\hat{H}_x)\tau} e^{4i\hat{H}_z\tau} e^{-i(\hat{H}_{xx}+4\hat{H}_x)\frac{\pi}{2}} e^{-4i\hat{H}_z\frac{\pi}{2}}, \\
&= e^{i(\hat{H}_{xx}+4\hat{H}_x)\tau} e^{4i\hat{H}_z\tau} = \hat{\mathscr{U}}_x^{\dagger}(\tau).
\end{aligned} \tag{4.15}$$

We see that the Floquet map at $(\frac{\pi}{2} - \tau)$ is a complex conjugate of the Flqouet map at τ. Therefore, OTOC behavior will be exactly the same at both τ and $(\frac{\pi}{2} - \tau)$. In the

integrable $\hat{\mathscr{U}}_0$ case, at $\tau = \frac{\pi}{18}$, dynamic region of the OTOC shows power-law growth with the exponent of the power-law $b = 2.03$ (approximately quadratic) [Fig. 4.2(a)]. In the range $\tau = 0$ to $\tau = \frac{\pi}{2}$, for any τ, OTOC shows power-law growth except at $\tau = \frac{\pi}{4}$. While approaching the saturation value, OTOC is not showing exponential behavior, as seen in the inset of Fig. 4.2(a). Let us check the behavior of OTOC by replacing the SBOs with random block operators (RBOs). With random block observables, OTOC thermalizes quickly as compared to SBOs. This led to the disappearance of power-law growth in the dynamic region for $\tau = \frac{\pi}{18}$. [Fig. 4.2(b)]. However, after the Ehrenfest time, the OTOC saturates exponentially with a rate $\mu = 0.14$ [Fig. 4.2(c)].

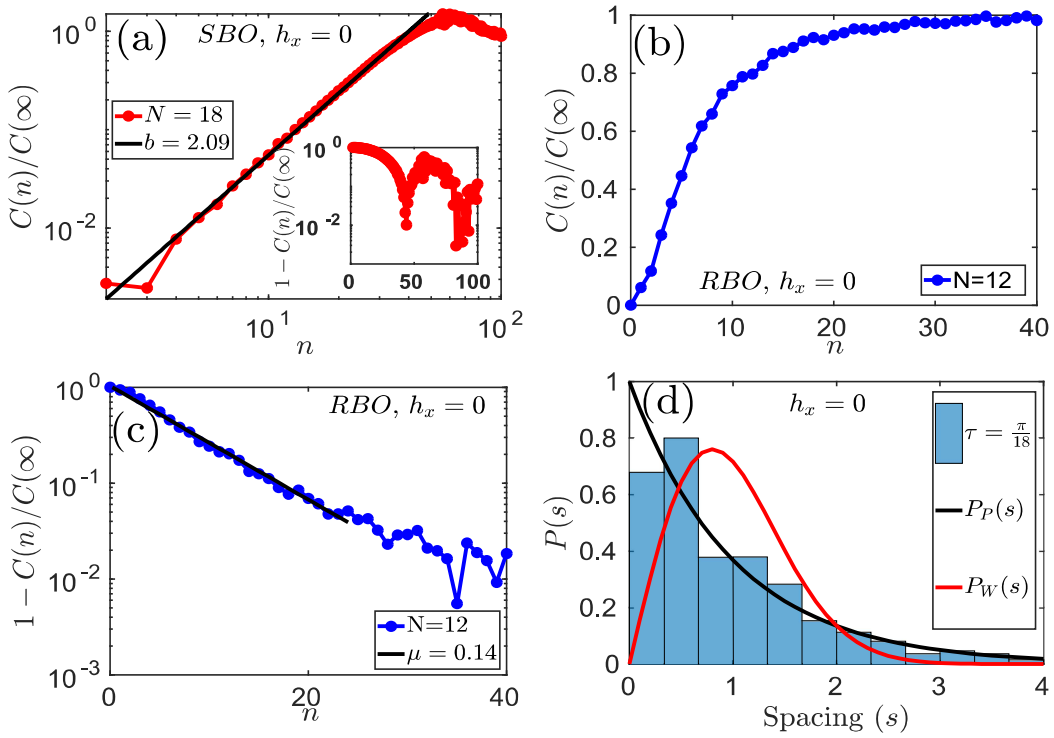

Fig. 4.2 Integrable $\hat{\mathscr{U}}_0$ system with parameters: $\tau = \frac{\pi}{18}$, $J_x = 1$, $h_x = 0$ and $h_z = 4$. (a) $C(n)/C(\infty)$ generated by SBOs vs. n for $N = 18$ (log $-$ log). Line with points represents data from the numerical calculation, and the solid line is the polynomial fitting. Inset shows $1 - C(n)/C(\infty)$ vs. n (log $-$ linear). (b) $C(n)/C(\infty)$ vs. n for $N = 12$ and RBOs as observables. (c) $1 - C(n)/C(\infty)$ vs. n for $N = 12$ and RBOs as observables. Line with points is data generated numerically, and a solid line is the exponential fitting. (d) NNSD for $N = 12$. In all the cases, open boundary condition is considered.

Fig. 4.2(d) shows the NNSD of the $\hat{\mathscr{U}}_0$ system at $\tau = \frac{\pi}{18}$ is Poisson type rather than Wigner-Dyson type [58, 62]. The system displays Poisson statistics at all the Floquet periods between 0 to $\frac{\pi}{2}$ except at $\frac{\pi}{4}$. At $\tau = \frac{\pi}{4}$, multiplication of the Floquet period and amplitude of the transverse magnetic field ($h_z\tau$) is equal to π resulting in a constant contribution of the field term in the Floquet map. Hence, for $\tau = \pi/4$, only the coupling term is present in the Floquet map, which provides degenerate eigenvalues. Due to this fact, NNSD is unable to specify the behavior of either the Poisson or Wigner-Dyson type. Mathematically, it can be given as:

$$\hat{\mathscr{U}_x} = e^{-i(\hat{H}_{xx}+4\hat{H}_x)\frac{\pi}{4}} e^{-4i\hat{H}_z\frac{\pi}{4}}, = e^{-i\hat{H}_{xx}\frac{\pi}{4}}. \tag{4.16}$$

OTOC in the nonintegrable $\hat{\mathscr{U}_x}$ system shows a power-law growth similar to that in the integrable case. However, in the $\hat{\mathscr{U}_x}$ case, the exponent of the power-law is smaller as compared to the integrable case. The exponent increases with increasing τ. At $\tau = \frac{\pi}{18}$ and $\frac{3\pi}{18}$ exponent of the power-law is 1.12 and 1.74, respectively. Hence, at $\tau = \frac{3\pi}{18}$, the exponent is nearly quadratic in a power-law growth [Fig. 4.3(a)]. The exponent of the power-law is independent of the system size, but the saturation of the OTOC depends on the system size. Longer the size, longer time it takes for saturation. Hence, the saturation value of OTOC exhibits the finite-size effect [Fig. 4.3(b)]. As $N \to \infty$, saturation will occur after the infinite number of kicks. OTOC reached to saturation exponentially at all the Floquet periods. As the Floquet period increases, the rate of saturation increases [Fig. 4.3(c)].

Now, if we replace the observables $\hat{V}$ and $\hat{W}$ to random matrices, growth of OTOC does not show Lyapunov or power-law type at any τ [Fig. 4.3(d)]. OTOC saturates exponentially, and the exponent of the exponential increases with increasing τ, which can be seen in Fig. 4.3(e).

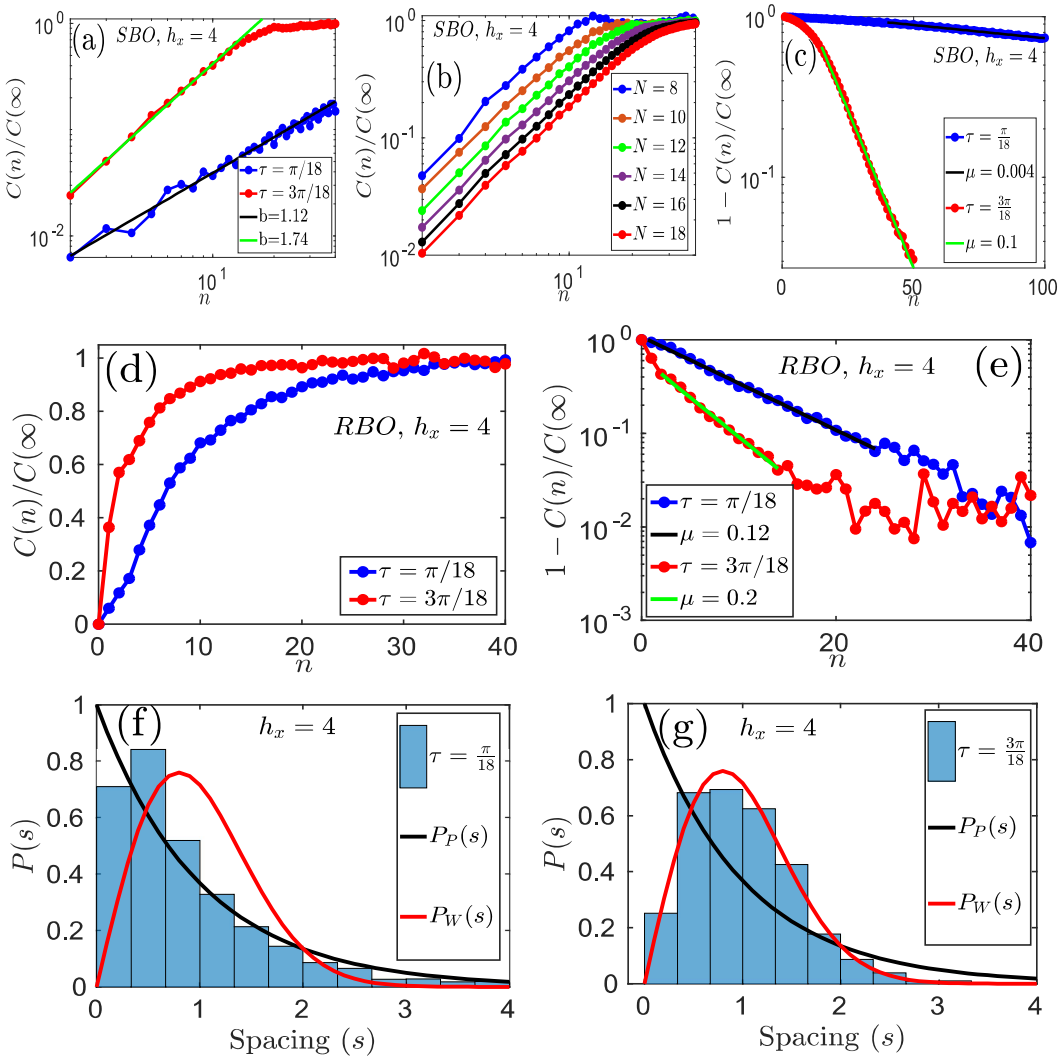

Fig. 4.3 Nonitegrable $\hat{\mathscr{U}}_x$ system with parameters: $J_x = 1$, $h_x = 4$, $h_z = 4$ and $\tau = \frac{\pi}{18}, \frac{3\pi}{18}$. (a) Illustrates the $C(n)/C(\infty)$ by using the SBOs vs. n for $N = 18$ (log − log). Lines with points represent data from the numerical calculation, and solid lines are the polynomial fitting with exponent $b = 1.12$ at $\tau = \frac{\pi}{18}$ and $b = 1.74$ at $\tau = \frac{3\pi}{18}$. (b) $C(n)/C(\infty)$ by using the SBOs vs. n at different N for $\tau = \frac{3\pi}{18}$. (c) $1 - C(n)/C(\infty)$ vs. n (log −linear). Lines with points are data generated numerically, and solid lines are the exponential fitting. (d) Illustrates the OTOCs of RBOs vs. n for $N = 12$ (g) $1 - C(n)/C(\infty)$ vs. n (log −linear). Lines with points are data generated numerically, and solid lines are the exponential fitting. NNSD of the $\hat{\mathscr{U}}_x$ system at (f) $\tau = \frac{\pi}{18}$ and (g) $\tau = \frac{3\pi}{18}$ with $N = 12$. In all cases, an open boundary chain is considered.

NNSD of the nonintegrable Floquet system displays the Wigner-Dyson distribution at Floquet period $\frac{\pi}{3}$ and crossover to the Poisson distribution as the Floquet periods changes away from the $\frac{\pi}{3}$. This point is the most chaotic point in the Floquet system [Fig. 4.3 (f, g)].

Floquet system at $\tau = \frac{\pi}{4}$ is a special case, which was reported in different contexts earlier as well [55, 186]. For the choice of parameters in this section *i. e.*, $h_x = 4$ and $h_z = 4$, and $\tau = \pi/4$ we get $h_{x/z}\tau = \pi$. This results in a constant contribution from the magnetic field terms in the Floquet map defined in subsection 4.2.1 and only the spin-spin interaction term $\hat{H}_{xx}$ term evolves the SBO in the OTOC calculation. Since the SBOs are also in the direction of spin-spin interaction *i.e.*, along the longitudinal direction, the SBO will be stationary at all times. Therefore, OTOC remains constant (equal to one) at all the kicks.

4.4 Special case

In the transverse Ising Floquet system, there is a peculiar set of parameters *viz.* $h_x = 0/1$, $h_z = 1$ and $\tau = \frac{\pi}{4}$ in both $\hat{\mathscr{U}}_0$ and $\hat{\mathscr{U}}_x$ systems. At this particular set of parameters, OTOC shows periodic oscillation in both integrable, as well as nonintegrable systems. In the integrable case, OTOC shows periodic behavior with a time period equal to $2N$. It jumps to a maximum value at $n = (2m+1)N$ and goes to zero at $n = 2mN$, where m is the positive integer and N is the system size [Fig. 4.4(a)]. OTOC shows quadratic growth till $N-1$ kicks [Fig. 4.4(b)]. Similar to the $\hat{\mathscr{U}}_0$ case, in the $\hat{\mathscr{U}}_x$ case, also OTOC shows a periodic behavior, but periodicity is not related to the system size [Fig. 4.4(c)]. Again, the OTOC grows quadratic [Fig. 4.4(d)]. Taking $\hat{V}$ and $\hat{W}$ as random matrices drawn from GUE, we do not see power-law growth of OTOC because spins in both the blocks are already thermalized before the time evolution starts. OTOC saturates exponentially in both $\hat{\mathscr{U}}_0$ and $\hat{\mathscr{U}}_x$ systems and for a given τ the exponent is nearly equal in both the cases ($\mu = 0.77$ for

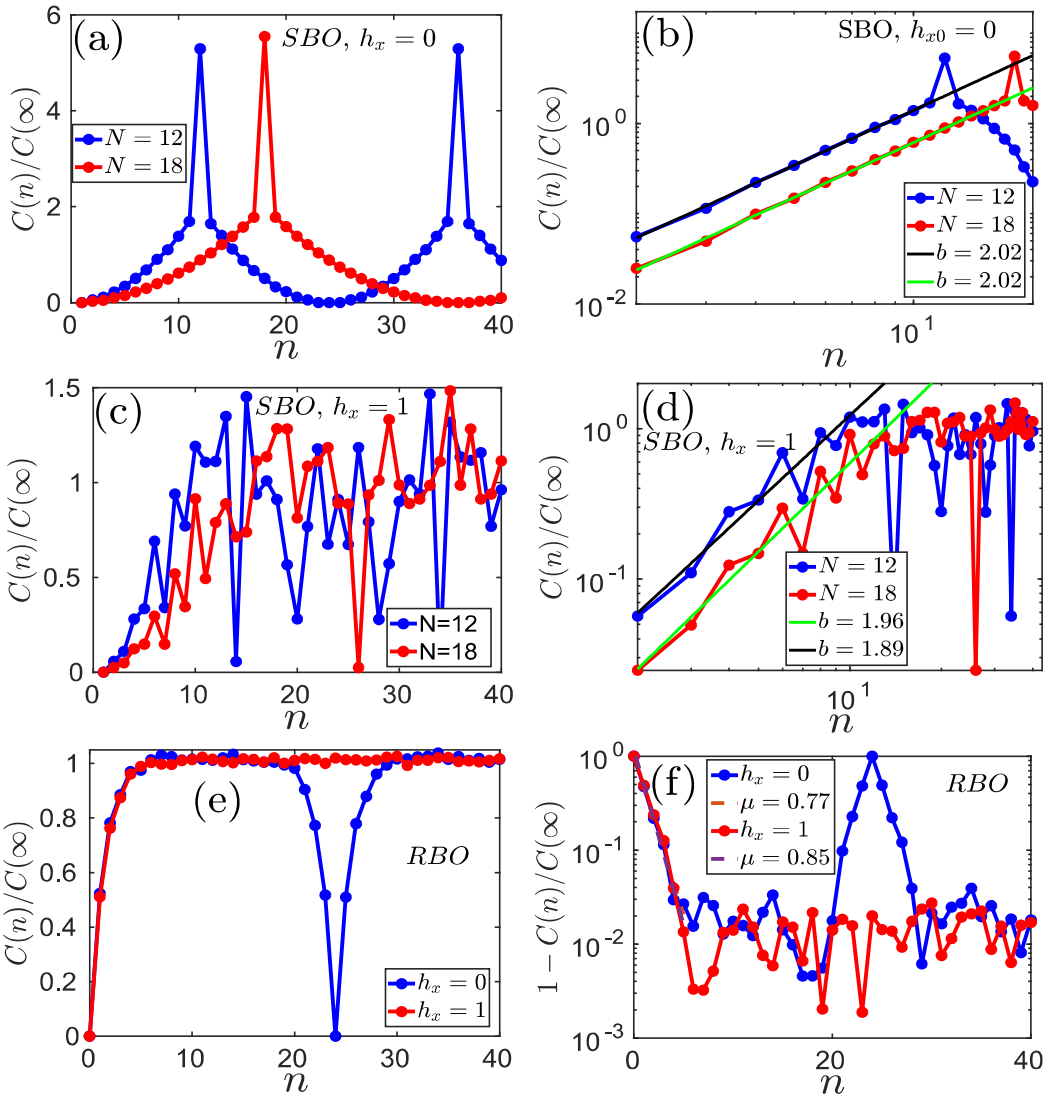

Fig. 4.4 (a) $C(n)/C(\infty)$ of SBOs vs. n in the $\hat{\mathscr{U}}_0$ system for $N = 18$. (b) $\log - \log$ behavior of "a" in which lines with points represent data from the numerical calculation, and solid lines are the polynomial fitting. (c) $C(n)/C(\infty)$ of SBOs with n in the $\hat{\mathscr{U}}_x$ system for $N = 18$. (d) $\log - \log$ behavior of "c" in which lines with points represent data from the numerical calculation, and solid lines are the polynomial fitting. (e) $C(n)/C(\infty)$ of RBOs vs. n in the $\hat{\mathscr{U}}_0$ and $\hat{\mathscr{U}}_x$ system for $N = 12$. (f) $1 - C(n)/C(\infty)$ vs. n for $N = 12$ ($\log -$ linear). Lines with points are data generated numerically, and solid lines are the exponential fitting. Other parameters: $J_x = 1$, $h_{0x} = 0/1$, $h_{0z} = 1$ and $\tau = \frac{\pi}{4}$. In all cases, an open boundary chain is considered.

$\tau = \frac{\pi}{18}$ and $\mu = 0.85$ for $\tau = \frac{3\pi}{18}$) as shown in Fig. 4.4(f). OTOC shows identical behavior to that of OPEE with time in both $\hat{\mathscr{U}}_0$ and $\hat{\mathscr{U}}_x$ systems (The equivalence is mathematically shown in Eq. (4.10). For the $\hat{\mathscr{U}}_0$ system, we see a periodic behavior with a time period equal to $2N\tau$. During this periodic behavior, OTOC starts from zero, goes to a maximum at N^{th} kick, and returns to zero at $t = 2N\tau$ and repeats the pattern thereafter. It should be noted that the entanglement entropy for the $\hat{\mathscr{U}}_0$ model with open boundary condition [157] and the entangling power of the $\hat{\mathscr{U}}_0$ model [186] is maximum at these points where OTOC is maximum. The reason lies to the fact that the OTOC at the infinite temperature is related to second Renyi entropy S_V^2 as $C(n) \sim e^{-S_V^2}$[11, 14], where $S_V^2 = -\log Tr_V(\rho_V^2)$, behaves like von Neumann entropy [11, 197]. $\rho_V = Tr_W[\rho]$ is the reduced density matrix for the partition scheme for the block operators defined in Fig. 4.1. At $n = 2mN$, where m is positive integer, due to quantum resonance [158], $\hat{W}(n = 2mN) = \hat{W}$ and the commutator $[\hat{W}(n = 2mN), V]$ becomes zero, therefore OTOC vanishes.

For this special set of parameters, the spectrum of the Floquet systems $\hat{\mathscr{U}}_0$ and $\hat{\mathscr{U}}_x$ are highly degenerate, and we could not conclude the nature of distribution from the shape of NNSD. We observe that a small shift in τ from $\pi/4$ lifts this degeneracy. Therefore, it is useful to explore the proximity of $\tau = \pi/4$ by defining a small parameter (let's say, $\varepsilon = \frac{\pi}{50}$) such that the natural behavior of NNSD and OTOC does not change by adding/subtracting ε to $\tau = \pi/4$. We explore not only NNSD but also OTOC at the proximity of $\tau = \frac{\pi}{4}$.

In the $\hat{\mathscr{U}}_0$ system with $\tau = \frac{\pi}{4} - \varepsilon$, we see OTOC deviates from the periodic behaviour at $\tau = \pi/4$. Though we still see maxima and minima of OTOC near $t = (2m+1)N\tau$ and $2mN\tau$ for positive integer m, respectively. We observe that smaller the ε, sharper the maxima/minima approaching to $t = (2m+1)N\frac{\pi}{4}/2mN\frac{\pi}{4}$ [Fig. 4.5(a)]. We again get a quadratic power-law growth at $\tau = \frac{\pi}{4} - \varepsilon$ [Fig. 4.5(b)]. Corresponding NNSD displays nearly Poisson statistics in the $\hat{\mathscr{U}}_0$ system [Fig. 4.5(c)].

On the other hand, OTOC in the $\hat{\mathscr{U}}_x$ system at $\tau = \frac{\pi}{4} - \varepsilon$ has different behaviour than that at $\frac{\pi}{4}$. At this period, OTOC grows till N kicks after that saturates at a value of 1 [Fig.

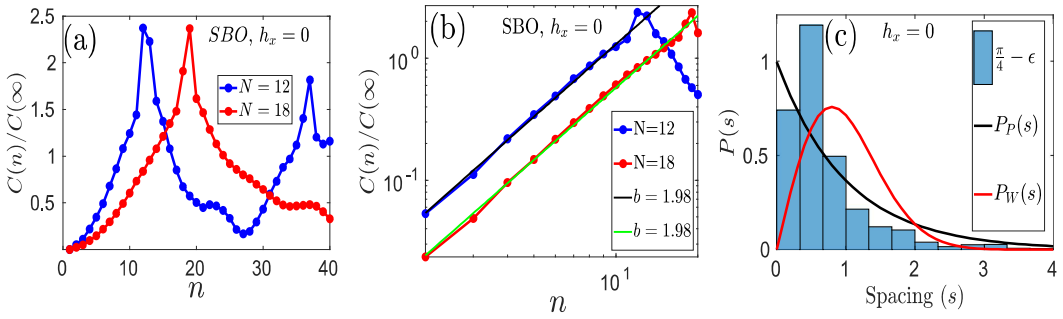

Fig. 4.5 Integrable $\hat{\mathscr{U}}_0$ system with parameters: $\tau = \frac{\pi}{4} - \varepsilon (= \frac{\pi}{50})$, $J_x = 1$, $h_x = 0$ and $h_z = 1$. (a) $C(n)/C(\infty)$ of SBOs vs. n in the $\hat{\mathscr{U}}_0$ system for $N = 18$. (b) log − log behavior of "a" in which lines with points represent data from the numerical calculation, and solid lines are the polynomial fitting. (c) NNSD of the $\hat{\mathscr{U}}_0$ system with $N = 12$.

4.6(a)]. Although the growth of OTOC is again quadratic power-law as shown in Fig. 4.6(b). Replacing the observable $\hat{V}$ and $\hat{W}$ by random matrices, we see the behavior of OTOC in both $\hat{\mathscr{U}}_0$ and $\hat{\mathscr{U}}_x$ system. We get a similar behavior of OTOC as that at $\tau = \frac{\pi}{4}$, in the $\hat{\mathscr{U}}_x$ system; however, in the $\hat{\mathscr{U}}_0$ system, OTOC does not reach to the value zero at $n = 2mN$. This is due to the parameter ε, which, if tending towards zero, leads to a coinciding $\tau = \pi/4 - \varepsilon$ case with $\tau = \pi/4$. Ideally, OTOC for RBOs should also vanish at $t = 2mN\pi/4$ due to the same reason that $\hat{W}(t = 2mN\pi/4) = \hat{W}$ but with $\tau = \pi/4 - \varepsilon$, we skip the moment of vanishing OTOC at $2mN$ kicks and get a dip only [Fig. 4.6(c)]. OTOCs with RBOs are identical to OPEE [Eq. 4.10]. Fig. 4.6(d) displays the exponential saturation of OTOC with nearly equal exponent in both $\hat{\mathscr{U}}_0$ and $\hat{\mathscr{U}}_x$ system. At period $\frac{\pi}{4} - \varepsilon$, there is no degeneracy in the spectrum. Therefore, NNSD shows Wigner-Dyson distribution [Fig. 4.6(e)].

4.5 Conclusion

In this chapter, we study the growth and saturation behavior of OTOC in both $\hat{\mathscr{U}}_0$ and $\hat{\mathscr{U}}_x$ systems. Initially, we calculated OTOC by using the SBOs for various time periods

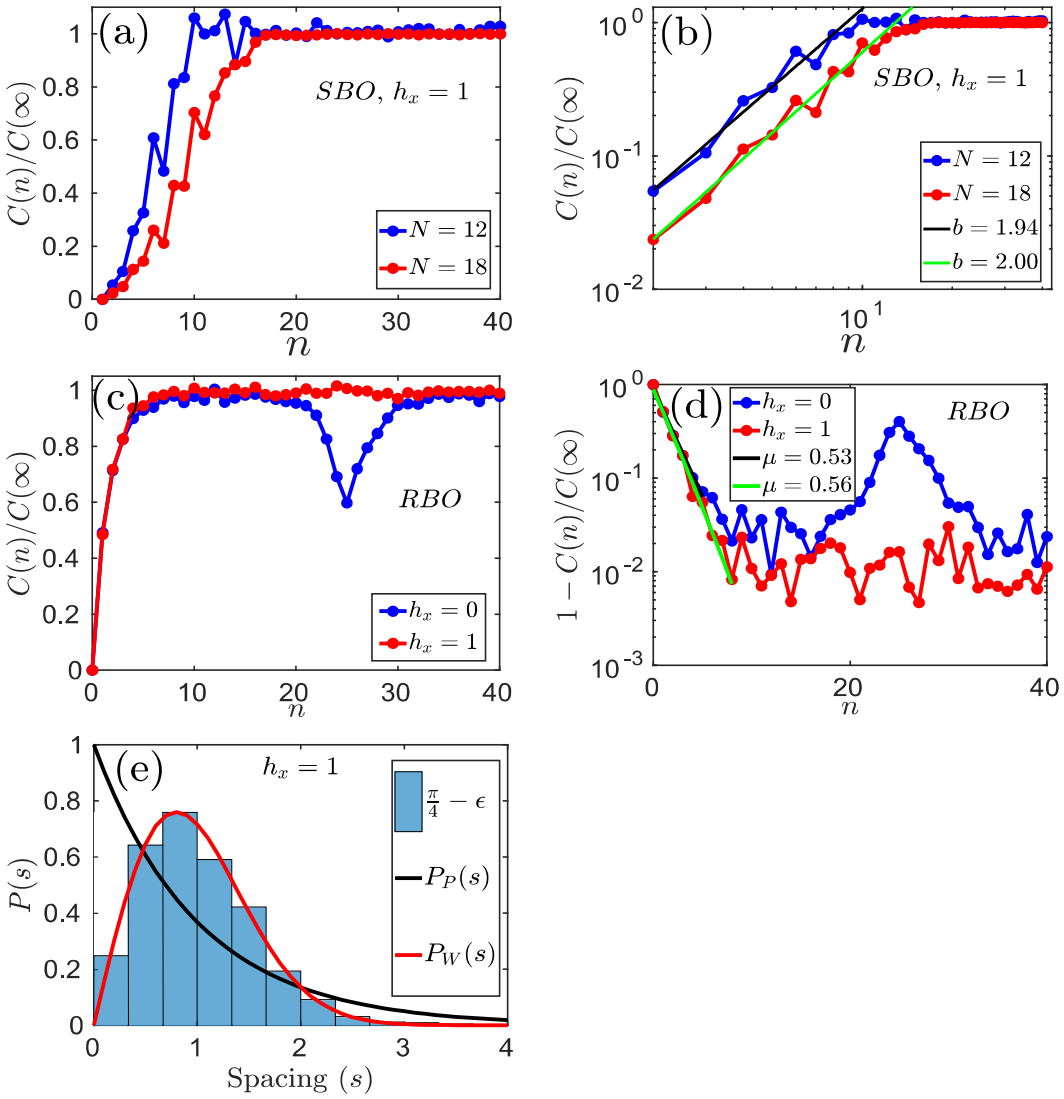

Fig. 4.6 (a) $C(n)/C(\infty)$ of SBOs vs. n in the $\hat{\mathscr{U}}_x$ system for $N = 12$ and 18. (b) $\log-\log$ behavior of "a" in which lines with points represent data from the numerical calculation, and solid lines are the polynomial fitting. (c) $C(n)/C(\infty)$ of RBOs vs. n in the $\hat{\mathscr{U}}_0$ and $\hat{\mathscr{U}}_x$ system for $N = 12$. (d) $1-C(n)/C(\infty)$ vs. n for $N = 12$ ($\log-$linear). Lines with points are data generated numerically, and solid lines are the exponential fitting. (e) NNSD of the $\hat{\mathscr{U}}_x$ system for $N = 12$. Other parameters: $J_x = 1$, $h_x = 0/1$, $h_z = 1$ and $\tau = \frac{\pi}{4} - \varepsilon (= \frac{\pi}{50})$.

and analyzed the early time behavior and saturation behavior. Later, we used analytically solvable RBOs to learn about the saturation region of the system.

Growth of OTOC in both $\hat{\mathscr{U}}_0$ and $\hat{\mathscr{U}}_x$ system shows a quadratic power-law for all Floquet periods in between 0 to $\frac{\pi}{2}$ except $\frac{\pi}{4}$. At kick interval $\tau = \frac{\pi}{4}$, the field terms do not change the state; therefore, OTOC remains constant.

Later we take special parameters ($J_x = 1$, $h_z = 1$, and $h_z = 0/1$ and $\tau = \frac{\pi}{4}$) and calculate the OTOC. In the integrable system, we see a periodic trend, and the period of oscillation is twice the system size. We also observe that the maxima/minima are those points where von Neumann entropy is also maxima/minima. In the nonintegrable case, periodic behavior does not show a trivial dependence on the system size. For $\tau = \pi/4$, OTOC shows a quadratic power-law growth in the integrable system till $n = N - 1$ kicks. We see a quadratic power-law for the nonintegrable system as well. Large degeneracy at $\tau = \frac{\pi}{4}$ makes NNSD inconclusive whether it is Poisson or Wigner-Dyson type. In order to study the behavior approaching to this Floquet period, we define a very small quantity (say $\varepsilon = \frac{\pi}{50}$) and take a slightly lesser Floquet period, $\tau = \frac{\pi}{4} - \varepsilon$. At this τ, NNSD is Poisson type in the $\hat{\mathscr{U}}_0$ system and Wigner-Dyson type in the $\hat{\mathscr{U}}_x$ system. We also studied the near-saturation behavior of OTOC. Near saturation behavior can not be exactly defined by using the SBOs; therefore, we calculate OTOCs by RBOs. For the observables in consideration, the OTOC with RBOs is exactly the same as the operator entanglement entropy. We are getting an exponential increase of OTOC near the saturation region in all the cases.

In the next chapter, we will utilize OTOCs as a quantifier for quantum information currents and propose a quantum information diode (QID) by exploiting the effect of nonreciprocal magnons in a 2D Heisenberg spin system with Dzyloshinski Moriya interaction.